

INTERNATIONAL DORIS SERVICE
I D S

Report of the 2003 Analysis Campaign
"Impact of GRACE gravity field models on IDS products"

M. Feissel-Vernier (1,2),

J.-J. Valette (3), L. Soudarin (3), K. Le Bail (2)

1. Observatoire de Paris/SYRTE
2. Institut Géographique National/LAREG
3. Collecte Localisation Satellites

May 2005

Report of the 2003 IDS Analysis Campaign

"Impact of GRACE gravity field models on IDS products"

Contents

1. Introduction	3
1.1 Purpose of the analysis campaign	3
1.2 Contributions	3
2. Analysis techniques used	5
2.1 Referencing times series of station coordinates (SINEX files) to ITRF2000	5
2.1.1 Analysis strategy	5
2.1.2 CATREF data modelling and analysis	7
2.2 Time series analysis	8
2.2.1 Extracting seasonal and low frequency components: the Crono_Vue algorithm.....	8
2.2.2 Allan variance	8
3. Analysis of series of terrestrial reference frames	9
3.1 Genealogy of the products analysed	9
3.2 Station coordinates consistency	10
3.3 Long time series of weekly terrestrial reference frames	12
3.3.1 Trend and interannual variations in the TRF origin and scale	13
3.3.2 Seasonal components	14
3.3.4 Stability.....	15
3.3.3 Differences in TRF origin and scale associated with the analysis environment	16
3.4 The Oct-Dec 2002 series of terrestrial reference frames	17
4. Analysis of orbital reference frames: origin and scale	18
4.1 The data analysed	18
4.2 Deterministic analysis of the differences	19
4.2.1 Bias	20
4.2.2 Local drift (over 90 days).....	21
4.2.3 Residual scattering	22
4.3 Spectral time analysis of differences	23
4.4 Global effects on the orbital and terrestrial reference frames	24
5. Summary: sensitivity to gravity field and to analysis environment	26
5.1 Short term internal consistency of station coordinates	26
5.2 Terrestrial reference frame sensitivity to the analysis context	26
5.3 Orbital reference sensitivity to the gravity field model used	27
6. Conclusion	28
<i>Annex 1. Allan variance response to simulated signals</i>	<i>29</i>
<i>Annex 2. References and acknowledgement</i>	<i>32</i>

1. Introduction

1.1 Purpose of the analysis campaign

The first gravity field models derived from the Grace mission were released in 2003. This new generation of gravity field models is expected to bring better accuracy and consistency in satellite geodesy applications, particularly for low orbiting satellites, hence for the IDS products. Taking the opportunity of the availability of these new models, the IDS organised an Analysis Campaign to investigate the impact of these new models on the IDS products.

The initial objective of the analysis campaign was to investigate the influence of the gravity field model used in DORIS data analysis on the derived terrestrial reference frames. Several Analysis Centers had volunteered to prepare a three-month time series of terrestrial reference frames referred to five different Earth gravity field models. The actual data that were available were less than expected in the sense that only one Analysis Center, LEGOS-CLS, provided this type of solution, but also more than expected, as three centers, IGN-JPL, INASAN and LEGOS-CLS provided long time series of terrestrial reference frames, starting in 1993, 1999 and 1993 respectively, and LEGOS-CLS provided three-month time series relative to the satellite orbits referred to various gravity field models.

This campaign takes place in the framework of the development of the IDS Analysis Coordination and intra-technique combination of products, a joint project of the Analysis Coordinator and the Central Bureau. Its purpose is two-fold:

- study in some detail the impact of the gravity field model used, not only on the precision of the results, but also on the stability of the reference frames, and
- develop tools for the comparison, validation and combination of terrestrial reference frames. For this reason, the analyses presented here make also use of other solutions available at the IDS Data Centers.

1.2 Contributions

The results considered for the analysis campaign fall into four categories, as follows.

1. Long series of SINEX files available at the IDS Data Centers over the period 1993-2004. The solutions considered are listed in table 1.1. Two of these solutions(ignwd03 and lcamd02) were already referred to ITRF2000 and partly analysed in the 2002 Analysis Campaign Report (see URL http://lareg.ensg.ign.fr/IDS/events/2002_camp_report.pdf). Further analyses of these data were performed for this report. **Note that the series analysed are those available at the end of 2004.** Figure 1.1 shows the improvement of the quality of results with the increase of number of satellites and the renovation of the stations.

Table 1.1. Long time series of TRF parameters since 1993, with solution names

Center	Gravity field models			Satellites
	EGM96	GRIM5-C1	GGM01C	
ign	ignwd03		ignwd05	Spot2, 4, 5, T/P, Envisat
lca		lcamd02		Spot2, 4, 3, T/P,

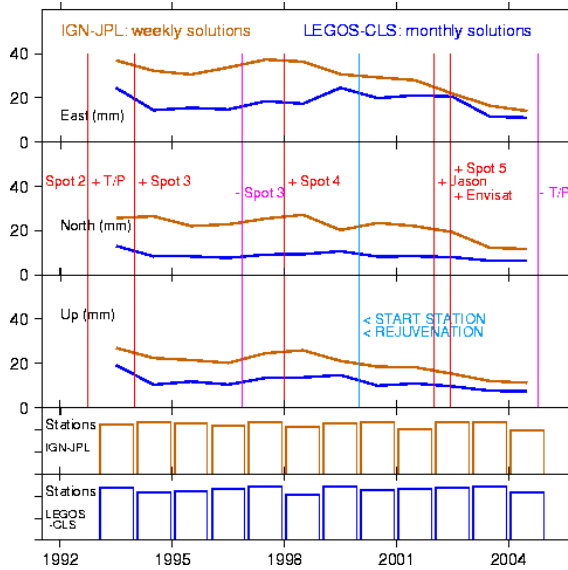


Figure 1.1. Evolution of the quality of DORIS positioning: median standard deviation of detrended series of station coordinates, computed year by year. Solutions: ignwd03 (weekly, brown) and lcamd02 (monthly, blue). The plotted parameters are the yearly median standard deviation of series of station coordinates determinations with respect to the linear trend estimated for the same year. The start and end dates of operation of the satellites are shown. The yearly numbers of stations with series of coordinates are shown at the bottom of the figure. The successive improvements associated with the increase in the number of satellites are visible.

- Series of coordinates of the geocentre and scale variation over 1999-2002, for satellites Spot2 and 4, and Topex/Poseidon (table 1.2).

Table 1.2. Weekly time series of TRF parameters

Center	Gravity field model
	JGM-3
ina	ina04wd01

- Global terrestrial frame results over the three months Oct-Nov-Dec 2002, for all satellites except Jason 1, using five gravity field models: two pre-GRACE models: EGM96, and GRIM5, and three models using the GRACE observations: GFZ01S (EIGEN-GRACE), GGM01S, and GGM01C. Jason 1 data were not used, to avoid mixing effects arising from the oscillator sensitivity to the South Atlantic Anomaly (SAA) radiation. The solutions received are listed in table 1.1. The ignwd solutions are extracted from the long series listed in table 1.3.

Table 1.3. Weekly time series of TRF parameters, with solution names

SINEX files, Oct-Dec 2002. Spot2, Spot4, Spot5, T/P, Envisat

Center	Gravity field models				
	EGM96	GRIM5-C1	GGM01C	GGM01S	EIGEN-GRACE01S
ign	ignwd03		ignwd05		
lca	lcawd06	lcawd07	lcawd08	lcawd09	lcawd10

- Orbit results over the three months Oct-Nov-Dec 2002, separately for all six satellites, using five gravity field models: two pre-GRACE models: EGM96 and GRIM5, and three models using the GRACE observations: GFZ01S (EIGEN-GRACE), GGM01S, and GGM01C. The latter is used as a reference in the comparisons. The solutions received consist of one-day

time series of the relative translation and scale parameters of the orbital reference frames. They are listed in table 1.4.

Table 1.4. Orbit results

Daily ephemerides comparisons by difference to GGM01C
Oct-Dec 2002. Spot2, Spot4, Spot5, T/P, Envisat, Jason1

Center	Gravity field models			
	EGM96	GRIM5-C1	GGM01S	EIGEN-GRACE01S
lca	[x]	[x]	[x]	[x]

2. Analysis techniques used

2.1 Referencing times series of station coordinates (SINEX files) to ITRF2000

2.1.1 Analysis strategy

The analysis of station positions is done using the common Helmert similarity of seven transformation parameters. SINEX files with full covariance matrices are checked and then combined with estimation of variance factors. A recommendation was done to the analysts to provide loose constraint solutions (sigma > 1 m on the station coordinates) or minimal constraint solutions.

The standard IDS request with respect to results submitted by the Analysis Centers is that one of the following three forms of constraints be used:

- Loose constraints: solutions where the uncertainty applied to the constraints is greater than 1 m for positions and greater than 10 cm/year for velocities. The constraint matrix in the SINEX block should be coded "SOLUTION/APRIORI".
- Removable constraints: solutions for which the estimated station positions and/or velocities are constrained to external values within an uncertainty around 10^{-5} m for positions and 10^{-6} m/year for velocities. In this case, the constraint matrix in the SINEX block should be coded "SOLUTION/APRIORI".
- Minimum constraints used solely to define the Terrestrial Reference Frame using a minimum amount of required information. For more details on the concepts and practical use of minimum constraints (see for instance Altamimi et al, 2001). The Analysis Center is invited to give details of how the method has been applied.

The analysis is based on the IGN/LAREG CATREF software (Altamimi et al, 2002), whose analysis structure is outlined in figure 2.1. For each time series of stations positions of a given solution, we have run CATREF in a global combination to estimate its internal consistency. First step is to remove uncertainties in the coordinate system associated to each solution and to express all of them in the same reference frame (datum definition). This step is done with the application of the minimum constraint equations without disturbing the underlying information. The datum definition makes use of a subset of reliable stations. The list used for this report is given in tables 2.1 and 2.2.

The combinations of time series were done independently for each series of tables 2.1 for the long time series and 2.2 for the Oct-Dec 2002 time span.

Table 2.2. List of stations used to refer the 1992-2004 series of solutions to ITRF2000

*CODE	PT	__DOMES__	T	_STATION DESCRIPTION_	APPROX_LON_	APPROX_LAT_	_APP_H_
ADEA	A	91501S001		ILE DES PETRELS antenn	140 00 05.1	-66 39 45.6	0.9
AREA	A	42202S005		AREQUIPA antenna	288 30 24.9	-16 27 56.6	2493.7
BADA	A	12338S001		BADARY antenna	102 14 05.7	51 46 11.0	812.3
CACB	A	41609S001		CACHOIERA PAULISTA ant	314 59 52.8	-22 40 57.8	571.1
CIBB	A	23101S001		CIBINONG antenna	106 50 55.8	-6 29 26.4	161.1
COLA	A	23501S001		COLOMBO	79 52 27.0	6 53 31.4	-76.8
DAKA	A	34101S004		DAKAR antenna	342 33 59.9	14 43 54.9	44.6
DIOA	A	12602S011		DIONYSOS antenna	23 55 58.3	38 04 42.2	513.6
DJIA	A	39901S002		DJIBOUTI antenna	42 50 47.9	11 31 34.7	716.0
EASA	A	41703S008		EASTER ISLAND antenna	250 36 58.8	-27 08 52.2	120.1
EVEB	A	21501S001		EVEREST antenna	86 48 47.3	27 57 29.3	4962.0
GALA	Z	42004S001		SAN CRISTOBAL antenna	270 23 01.6	-0 54 02.5	5.3
GOMB	A	40405S037		GOLDSTONE antenna	243 12 29.1	35 14 54.1	1041.1
GUAB	A	50501S001		GUAM antenna	144 54 50.4	13 32 23.0	290.9
KERB	A	91201S003		KERGUELEN antenna	70 15 45.7	-49 21 07.5	62.6
KOKA	A	40424S008		KAUAI antenna	200 20 04.7	22 07 23.2	1165.7
KRUB	A	97301S004		KOUROU antenna	307 21 36.7	5 05 55.0	109.8
MANA	A	22006S001		MANILLE antenna	121 02 28.2	14 32 07.6	87.0
META	A	10503S013		METSAHOVI antenna	24 23 04.2	60 14 31.2	62.9
NOUA	A	92701S001		NOUMEA antenna	166 24 37.4	-22 16 10.1	85.3
PURA	A	21604S003		PURPLE MOUNTAIN antenn	118 49 29.3	32 04 01.7	263.5
RIDA	A	40499S016		RICHMOND	279 36 39.7	25 37 25.4	-18.5
ROTA	A	66007S001		ROTHERA antenna	291 52 32.2	-67 34 09.5	26.9
TRIA	A	30604S001		TRISTAN DA CUNHA ant.	347 41 14.9	-37 03 55.0	48.6
WALA	A	92901S001		WALLIS antenna	183 49 13.9	-13 15 56.7	158.9
YELA	A	40127S007		YELLOWKNIFE antenna	245 31 11.6	62 28 51.3	186.4

Table 2.2. List of stations used to refer the Oct-Dec 2002 series of weekly solutions to ITRF2000

*CODE	PT	__DOMES__	T	_STATION DESCRIPTION_	APPROX_LON_	APPROX_LAT_	_APP_H_
KIUB	A	12334S006		KIUBB antenna	66 53 07.3	39 08 05.0	623.4
PURA	A	21604S003		PURPLE MOUNTAIN antenn	118 49 29.3	32 04 01.7	263.5
MANA	A	22006S001		MANILLE antenna	121 02 28.2	14 32 07.6	87.0
YELB	A	40127S008		YELLOWKNIFE antenna	245 31 12.5	62 28 51.9	182.0
GOMB	A	40405S037		GOLDSTONE antenna	243 12 29.1	35 14 54.1	1041.1
KOKA	A	40424S008		KAUAI antenna	200 20 04.7	22 07 23.2	1165.7
RIDA	A	40499S016		RICHMOND	279 36 39.7	25 37 25.4	-18.5
CACB	A	41609S001		CACHOIERA PAULISTA ant	314 59 52.8	-22 40 57.8	571.1
SANB	A	41705S009		SANTIAGO	289 19 52.9	-33 08 58.6	724.5
GALA	Z	42004S001		SAN CRISTOBAL antenna	270 23 01.6	-0 54 02.5	5.3
MORB	A	51001S002		PORT MORESBY antenna	147 11 11.6	-9 26 02.4	118.4
ROTA	A	66007S001		ROTHERA antenna	291 52 32.2	-67 34 09.5	26.9
KESB	A	91201S004		KERGUELEN antenna	70 15 19.6	-49 21 06.1	74.4
ADEB	A	91501S002		ILE DES PETRELS antenn	140 00 07.3	-66 39 54.6	-1.0

2.1.2 CATREF data modelling and analysis

For a given Analysis Center, the input is a time series of station positions and associated variance-covariance matrices: X_s^i, Σ_s^i . The general combination model is based on the following equation:

$$X_s^i = X^i + (t_s^i - t_0) \cdot \dot{X}^i + T_k + D_k \cdot X^i + R_k \cdot \dot{X}^i$$

where t_s^i is the epoch of station i available in solution s and t_0 is chosen to be the median epoch of the incorporated solutions. T_k, D_k, R_k are estimated translation, scale factor and rotation, where k is the frame associated to the solution s . X^i, \dot{X}^i : combined solution at t_0 .

The normal equation constructed using the above model is singular, having a rank deficiency of 14, corresponding to the datum definition parameters. In order to define the combined frame an equation of minimum constraints is used, given by:

$$(A^T A)^{-1} A^T (X_R - X_E) = 0$$

where X_E is the vector of estimated station positions and velocities, X_R is the reference solution containing a selected set of stations and A is the design matrix of partial derivatives. Unlike the classical constraints applied over station coordinates, minimum constraints are applied over the frame parameters, thus allowing to express the combined solution in any external frame (e.g. ITRF2000), without altering the quality (or internal consistency) of the estimated solution. For more details, see (Altamimi et al., 2002) and (Sillard et al. 2001). The variance analysis is based on a variance factor estimation for each solution after the combination, as specified in (Altamimi et al., 2002).

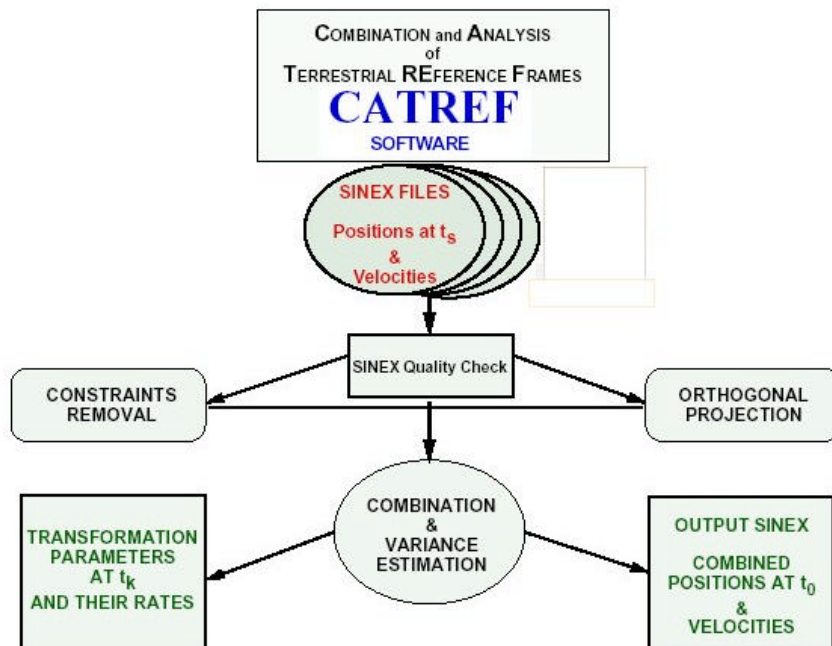


Figure 2.1. Analysis structure of the CATREF software package

2.2 Time series analysis

After CATREF software combination of the time series as explained in section 2.1, the outputs for each of the time series are as follows:

- Combined solution in positions and velocities at the date corresponding to the middle of the whole data span,
- Time series of coordinates expressed in ITRF2000, for each solution, at the date corresponding to the middle of the data span,
- Time series of residual coordinates relative to the combined solution,
- Time series of the Helmert transformation parameters for each solution, relative to the combined solution.

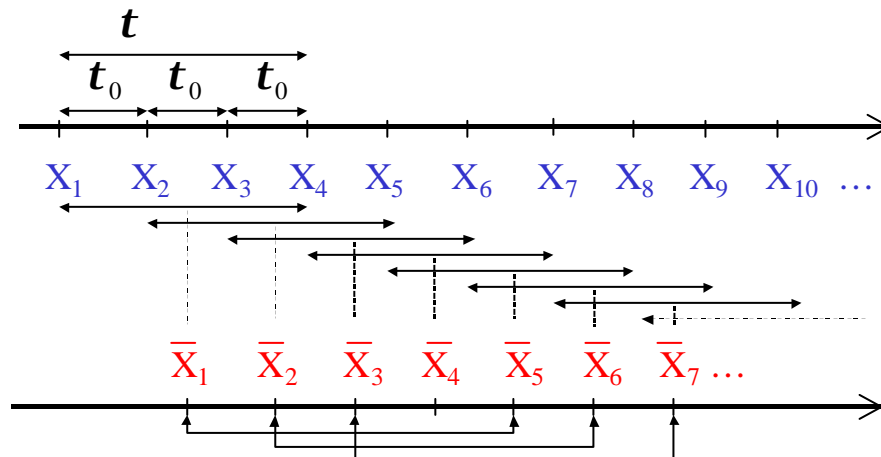
They are submitted to various analyses, such as extraction of a seasonal component when the series encompasses several years, scattering estimation, stability diagnosis by means of the Allan variance analysis. We give hereafter some details on the methods used.

2.2.1 Extracting seasonal and low frequency components: the Crono_Vue algorithm

Crono_Vue is a time series visualising tool. It extracts from the time series various components, such as trend (low frequency component), cyclic and irregular components. It also analyses the spectral content and performs Allan variance stability analyses. The main output is graphical. Crono_Vue is coded in Fortran and uses the GMT graphical package in a UNIX environment. It makes use of a few classical statistical concepts that the reader will find in the papers listed in the references. The software source as well as examples of applications are available through URL <http://lareg.ensg.ign.fr/IDS/software.html>.

2.2.2 Allan variance

The Allan (1966) variance may be defined as follows. Let us consider a stochastic process $(X_j)_{j=1,N}$ whose realisations X_j are available at a constant time interval time t_0 . For a sampling time t (t being a multiple of t_0 : $t = Mt_0$), we split the measurement time span into sub-samples with length t and we write the measurement as $(X_k)_{k=i,i+M-1}, i \in \{1, N - M + 1\}$.



The average value over these sub-samples is :

$$\bar{X}_{l,M} = \frac{1}{M} \sum_{i=l}^{l+M-1} X_i \quad , \quad l \in \{1, N - M + 1\} \quad , \quad \text{with } M = \frac{t}{t_0} .$$

The Allan variance for the sampling time t is then defined by

$$s_X^2(t) = \frac{1}{2} E[(\bar{X}_{k+M,M} - \bar{X}_{k,M})^2] \quad , \quad \text{with } M = \frac{t}{t_0} .$$

The Allan variance can then be estimated by

$$\hat{s}_X^2(t) = \frac{1}{2 \left(N - 2 \left(\frac{t}{t_0} \right) + 1 \right)} \sum_{k=1}^{N - 2 \left(\frac{t}{t_0} \right) + 1} (\bar{X}_{k + \frac{t}{t_0}, \frac{t}{t_0}} - \bar{X}_{k, \frac{t}{t_0}})^2$$

The Allan variance analysis (see a review of these methods in Rutman (1978)) allows one to characterise the power spectrum of the variability in time series, for sampling times ranging from the initial interval of the series to 1/4 to 1/3 of the data span, in our case one year through four years. This method allows one to identify white noise (spectral density S independent of frequency f), flicker noise (S proportional to $1/f$), and random walk (S proportional to $1/f^2$). Note that one can simulate flicker noise in a time series by introducing steps of random amplitudes at random dates. In the case of a white noise spectrum (an implicit hypothesis in the current ICRF computation strategy), accumulating observations with time eventually leads to the stabilisation of the mean position. In the case of flicker noise, extending the time span of observation does not improve the quality of the mean coordinates. A convenient and rigorous way to relate the Allan variance of a signal to its error spectrum is the interpretation of the Allan graph, which gives the changes of the Allan variance for increasing values of the sampling time t . In logarithmic scales, slopes -1 , 0 and $+1$ correspond respectively to white noise, flicker noise and random walk.

The main characteristics of the response of the Allan variance to simulated signals with known spectrum are shown in Annex 1.

3. Analysis of series of terrestrial reference frames

The global terrestrial frame results are analysed over a long period (§3.3) and over the three months Oct-Nov-Dec 2002 (§3.4). They are analysed according to their specific time spans.

3.1 Genealogy of the products analysed

The data analysis strategy and modelling that was used by the contributors are described in the following files, available from the two IDS Data Centers at CDDIS and IGN.

- ign: .../doris/products/sinex_series/ignwd/ignwd03.snxdsc (EGM96)
 .../doris/products/sinex_series/ignwd/ignwd05.snxdsc (GGM01C)
- ina: .../doris/products/geoc/ina04wd01.geoc.dsc
- lca: .../doris/products/sinex_series/lcamd/lcamd02.snxdsc
 .../doris/products/2003campaign/lcawd/lcawd01_snx_dsc - lcawd05_snx_dsc

The main characteristics relevant to this study are as follows.

- Satellites
 - o Spot 2, Spot 4, Topex/Poseidon
 - o Spot 5, Envisat (except in ina04dw01)
 - o Jason 1 data are used only in the lcamd02 solution

- References
 - o ITRF2000 (see section 2.1)
 - o Reference epoch. ign: 1 Jan 1986 ina: 1997.0 lca: 1997.0
 - o Gravity fields complete to degree and order: ign: 120, 120 ina: 70, 70 lca: 95, 95

- Analysis conditions and modelling
 - o Elevation cutoff. ign: as provided in the data (12° or lower, depending on the site and the satellite) ina: 18° lca: 12°
 - o Orbit length. ign: 1 day; ina: 30 hours; lca: 1 day, except T/P (~3 days)
 - o Tidal corrections applied: solid Earth tide; pole tide and ocean loading
 - o Atmospheric loading correction: applied only by lca
 - o Satellite center of mass - phase center correction applied
 - o Satellite attitude correction applied for T/P, Jason 1 and Envisat
 - o Spot orientation assumed geocentric
 - o Receiver-antenna phase center correction

- Estimated geodetic parameters:
 - o Cartesian station coordinates
 - o Daily pole coordinates. Pole coordinates rates estimated by ign only
 - o Daily UT1-UTC and rate estimated by ign and ina only
 - o Orbit: initial position and velocity

- Other estimated parameters:
 - o Solar radiation pressure. ign, lca: one coefficient/arc ; ina : stochastic variations
 - o Atmospheric drag. Estimated by ign and lca only
 - o Empirical acceleration parameters. Estimated by ign and lca only
 - o Tropospheric zenith path delay per pass and per station
 - o Frequency offset per pass and per station

The results are under the form of time series of weekly values of the origin of the TRF relative to ITRF2000, and of scale.

3.2 Station coordinates consistency

The combination of individual series for each Analysis Center provides the internal consistency of the solutions. Results are analysed in terms of transformation parameters and stations residuals. The plots in figure 3.1 show the weighted rms station coordinate residuals for the Grace Oct-Dec. 2002 campaign and for the 1993-2004 long time series. **The GGM01S GRACE Earth's gravity field model provides the best consistency of station coordinates** for the Sinex samples considered in the campaign, with a level of weekly weighted rms residuals (wrms) under 15 mm. Figure 3.2 shows **the influence of the number of satellites tracked on the combination consistency**. The wrms station coordinate residual falls under 15 mm as soon as five satellites are available in 2002 (Topex, Spot2-4-5 and Envisat).

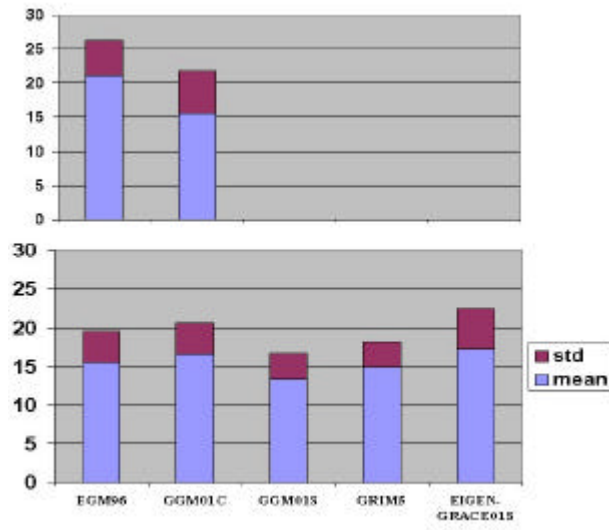


Figure 3.1. Oct-Dec 2002 Grace campaign. The mean weekly weighted rms station residuals and standard deviation over the three months are shown for the various gravity field models. Up: ign, bottom: lca.

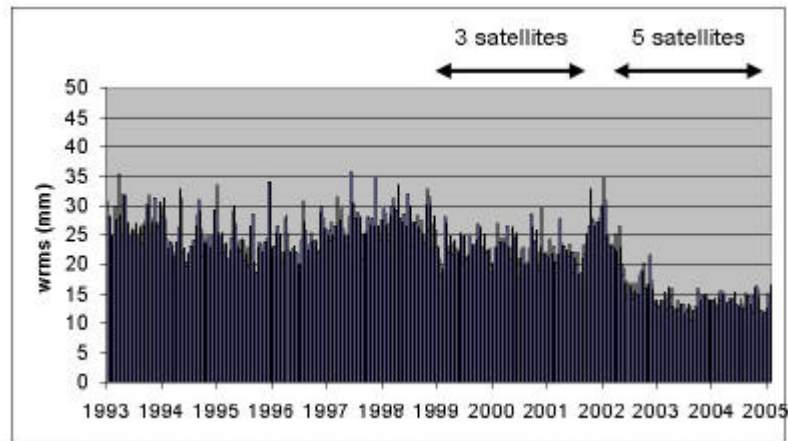


Figure.3.2. 1993-2004 weekly weighted rms of the station residuals (ignwd03 solution)

3.3 Long time series of weekly terrestrial reference frames

The time series of the coordinates of TRF origin and of the scale are submitted to the Crono_Vue algorithm described in section 2 for extracting the seasonal, interannual and long term components. An example of the Crono_Vue out put is given in figure 3.3.

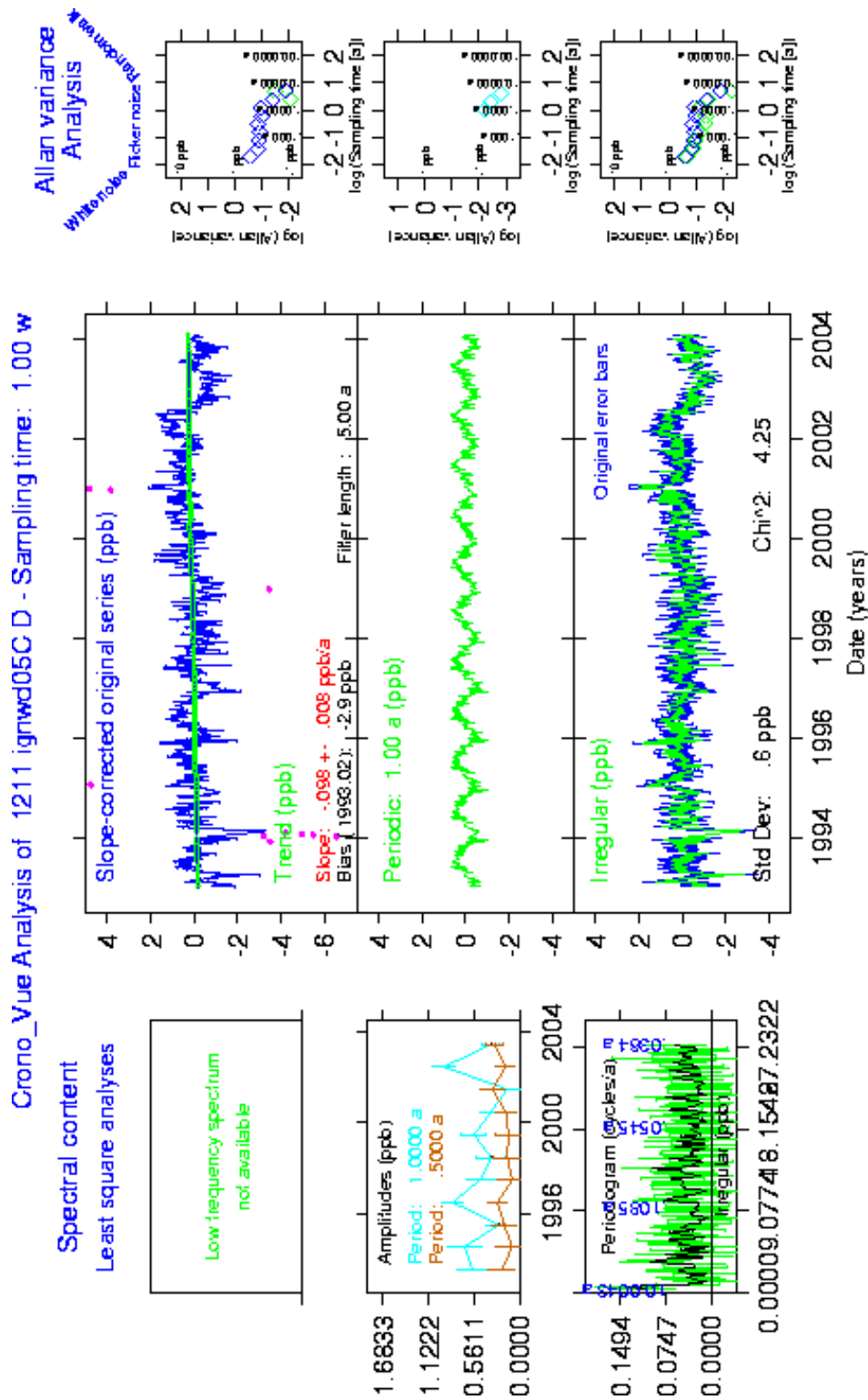


Figure 3.3. Crono_Vue signal decomposition of the series of scale parameters of ignwd05. The original series is shown in blue in the upper central frame, with outliers in pink and trend in green. The annual component is shown in the middle frame, and the residuals in the lower frame.

3.3.1 Trend and interannual variations in the TRF origin and scale

The main characteristics of the signal decomposition are given in tables 3.1 for the TRF origin and 3.2 for the scale. Figure 3.4 shows the low frequency (non linear trend and interannual) components of the time series of coordinates of the TRF origin with respect to ITRF2000. The solutions ignwd03 and ignwd05, that are respectively referred to EGM96 and GGM01C show very similar long term trends (left part of the figure). Quite larger discrepancies exist between the various solutions, in particular_lcamd02 in Y and ina04w01. We conclude that **the effect of the gravity field on the long term TRF origin motion is negligible when compared to the cumulative effect of analysis differences**. The situation of the interannual variations is similar, except for time-varying differences up to 4 mm in Z associated with the change of gravity field in the ign solutions.

Table 3.1. Components of the TRF origin motion relative to ITRF2000

Series	Bias (1997.0)			Linear trend			wrms residual*		
	Tx	Ty	Tz	Tx	Ty	Tz	Tx	Ty	Tz
	(mm)			(mm/year)			(mm)		
ignwd03	- 3.0	12.8	- 12.8	- 1.15	0.70	4.59	6.2	6.5	18.8
ignwd05	- 2.5	12.4	- 13.0	- 0.76	0.57	4.46	6.3	6.6	18.7
ina04wd01	+ 14.6	9.0	14.6	- 2.57	- 1.47	- 1.82	10.8	9.0	45.8
lcamd02	- 3.9	- 1.8	- 5.0	- 0.47	- 0.53	4.94	4.6	4.4	14.2

* After taking out also the seasonal component, except for ina04wd01

Table 3.2. Components of the scale variations relative to ITRF2000

Series	Bias (1997.0)	Linear trend	wrms residual*
	(ppb)	(ppb/year)	(ppb)
ignwd03	- 3.3	- 0.09	0.6
ignwd05	- 3.3	- 0.10	0.6
ina04wd01	- 3.9	+ 0.17	1.7
lcamd02	+ 3.1	- 0.37	0.7

* After taking out also the seasonal component, except for ina04wd01

The scale results shown in table 3.4 and figure 3.5 show **insignificant scale differences associated with the change of gravity field in the ign solutions, but remarkable discrepancies in level and slope between the ign and lca solution**.

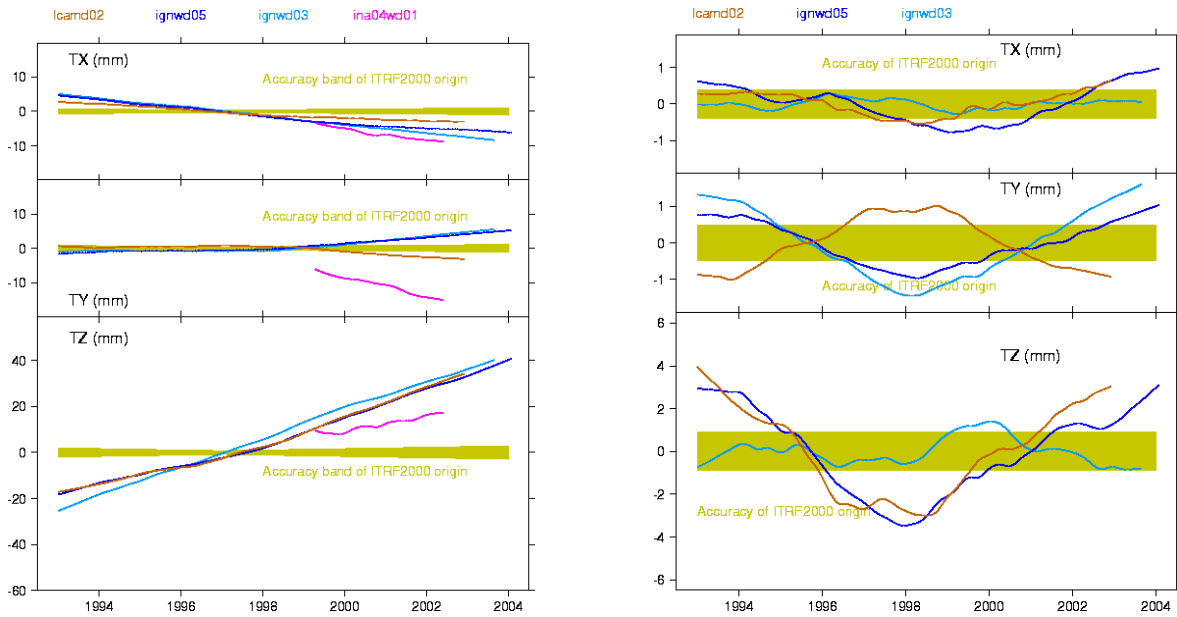


Figure 3.4. Trend (left part) and interannual variations (right part) of the coordinates of the TRF origin relative to ITRF2000.

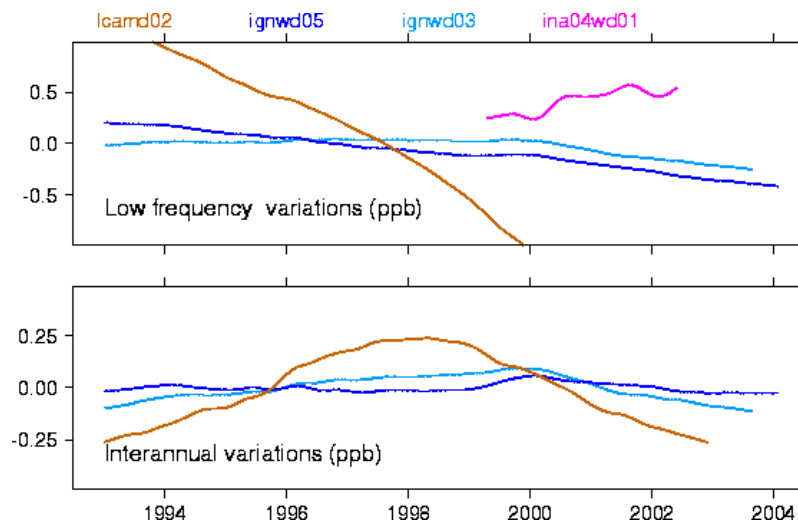


Figure 3.5. Trend (upper part) and interannual variations (lower part) of the TRF scale relative to ITRF2000.

3.3.2 Seasonal components

Figure 3.6 shows the annual components of the TRF origin and scale variations of the compared solutions. The TRF origin variations predicted from the geophysical excitation over 1993-1999 are also shown (Feissel-Vernier et al. 2004). **They show insignificant differences associated with the change of gravity field in the TRF origin variations and a reasonable agreement in phase and amplitude with the geophysical prediction in the equatorial plane. However, the amplitude of the geodetic signal, especially in TX, is varying with time, while the geophysical prediction is not.** By construction, the amplitude of the annual geophysical excitation is expected to be stable, but this may not necessarily be realistic.

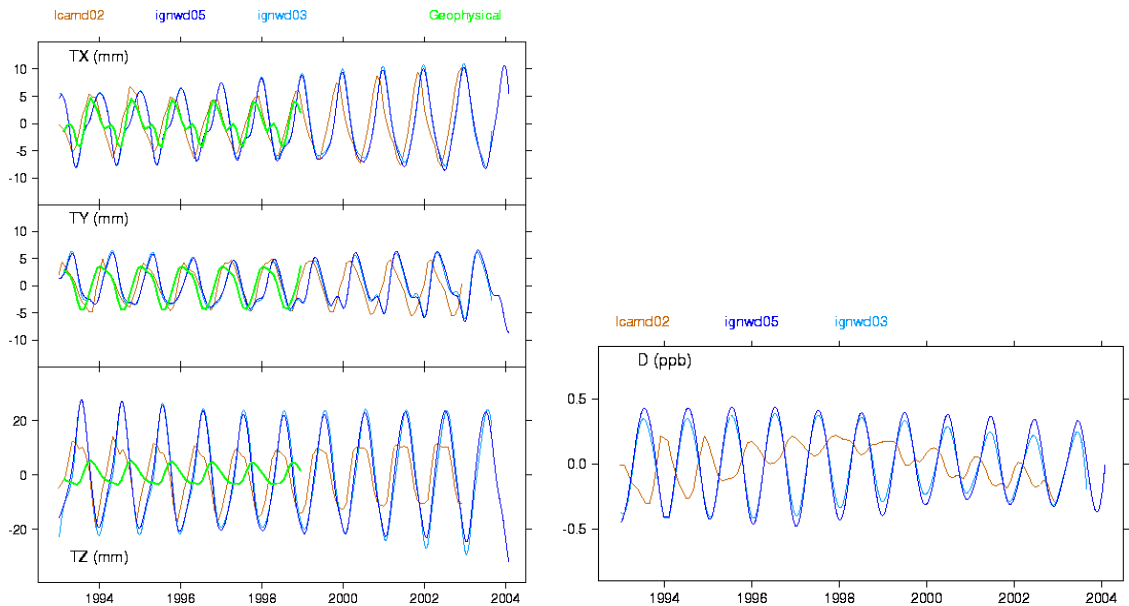


Figure 3.6. Annual components of the TRF origin and scale variations.

3.3.4 Stability

Figure 3.7 shows the behaviour of the DORIS and geophysical TRF origin motions under a spectral viewpoint, using the Allan graph description. The four DORIS solutions have similar signatures in the equatorial plane components: the seasonal signature is imbedded in a noise with a spectrum close to white noise. The Tx and Ty components reach a stability of 2-3 mm for a one-year sampling time. The spectrum of the Tz variations is quite noisier than those in the equatorial plane, with a stability of 2-3 cm for a one-year sampling time. In all three components the spectral power of the DORIS signal remains higher than that of the geophysical one.

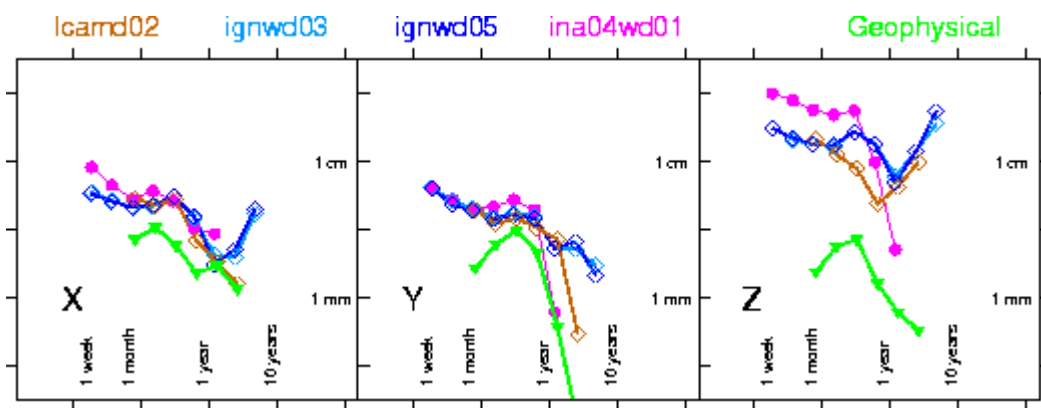


Figure 3.7. Spectral signature of geocenter motion observed with DORIS and expected from geophysical data. Colour code: light blue: ignwd03; blue: ignwd05; pink: ina04wd01; brown: lcamrd02; green: geophysical. A slope equal to -1 is the signature of white noise.

Figure 3.8 shows the spectral behaviour of the TRF scale time series. The IGN series has a higher level of noise in the short term, and the LCA a higher noise level in the long term. The

annual component signatures are barely visible in the noise context. The scale reaches a stability of 0.2-0.6 ppb for a one-year sampling time.

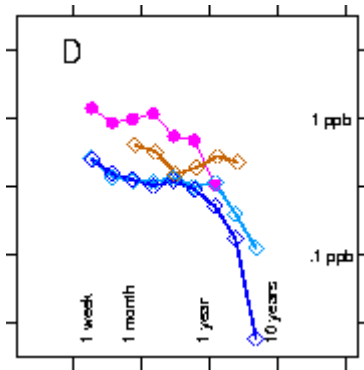


Figure 3.8. Spectral content of DORIS time series of TRF scale. Colour code: light blue: ignwd03; blue: ignwd05; pink: ina04wd01; brown: lcamd02. A slope equal to -1 is the signature of white noise.

3.3.3 Differences in TRF origin and scale associated with the analysis environment

The discrepancies between solutions that can be ascribed to gravity field differences or to other causes are summarized in table 3.3.

Table 3.3. Components of the scale variations relative to ITRF2000

	----- Influence of -----		
	Gravity field	Datum definition	Software & Analyst
Origin (Equatorial)			
Annual amplitude	1 mm	1 mm	5 mm
Interannual	1 mm	1 mm	3 mm
Trend	0.4 mm/a	1 mm/a	1.5 mm/a
Origin (Axial)			
Annual amplitude	1 mm	10 mm, variable	15 mm
Interannual	4 mm	4 mm	4 mm
Trend	0.1 mm/a	0.2 mm/a	6 mm/a
Scale			
Annual amplitude	0.1 ppb	0.3 ppb, variable	0.5 ppb, var.
Interannual	0.05 ppb	0.05 ppb	0.25 ppb
Trend	0.01 ppb/a	0.05 ppb /a	0.6 ppb /a

3.4 The Oct-Dec 2002 series of terrestrial reference frames

Figures 3.9 and 3.10 show the three-month time series of the translations and scale based on various gravity field models, derived by *lca* and *ign* respectively.

The translations slopes in the *lca* solutions are similar for GRIM5-C1 and EIGEN-GRACE01S. translations referred to EGM96 have relative slopes at the 10-20 mm/year level. The slope differences for EGM96 relative to GGM01C are slightly smaller in the *ign* translations. The translations detrended standard deviations, that express the short-term scattering, are insensitive to the gravity field models. They are at the 5-6 mm level in the equatorial plane and at the 8-9 mm level in T_z .

For the scale, the *lca* values relative to EIGEN-GRACE01S differ by 11 and 9 ppb/year for EGM96 and GRIM5-C1, respectively. The difference in scale slope in the two *ign* solution (EGM96 and GGM01C) is only 1 ppb/year. The spectral signatures (Allan graphs) are unaffected by the change of gravity field model.

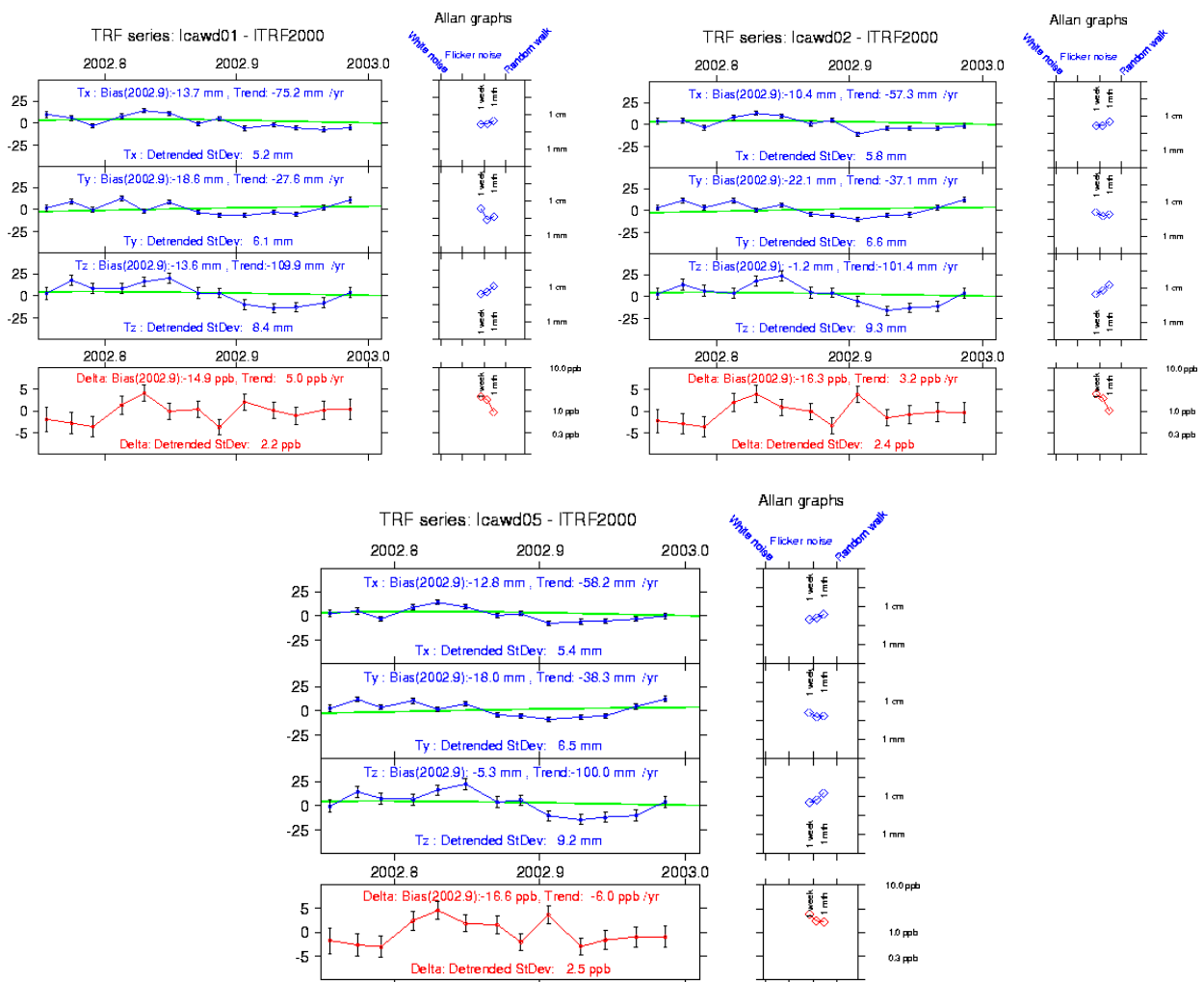


Figure 3.9. Weekly translations (blue curves) and scale (red curves) relative to ITRF2000 over Oct-Dec 2002. *lca* analysis. The reference gravity field models are, up left and right: EGM96, GRIM5-C1 respectively, bottom: EIGEN-GRACE01S. The green line shows the geophysically-expected geocenter motion. Note: series lcawd01, 02, and 05 correspond to lcawd06, 07, and 10 respectively.

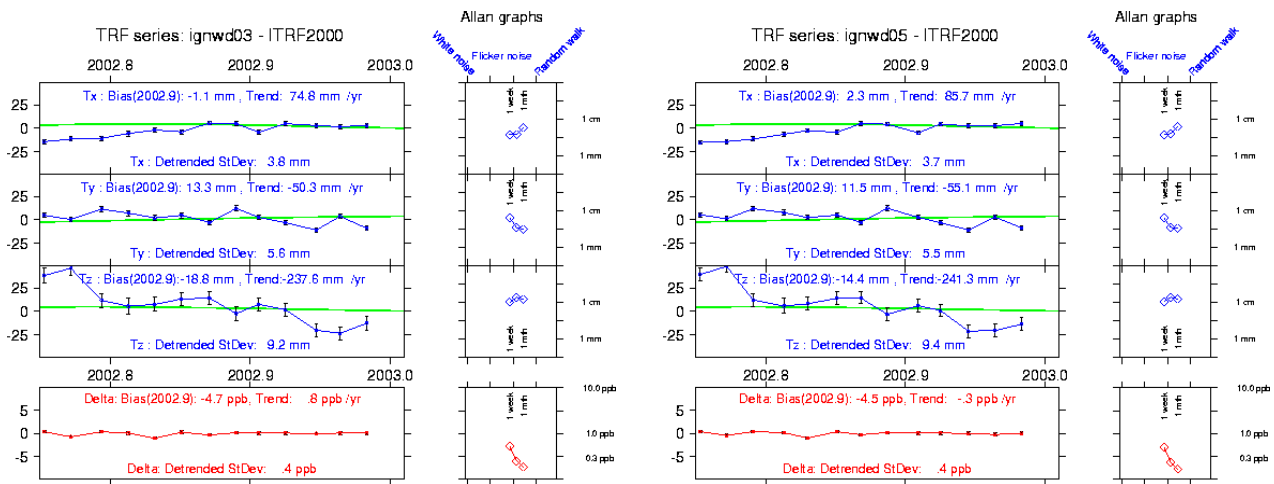


Figure 3.10. Weekly translations (blue curves) and scale (red curves) relative to ITRF2000 over Oct-Dec 2002. **ign** analysis. The reference gravity field models are, from left to right: EGM96, GGM01C. The green line shows the geophysically-expected geocenter motion.

4. Analysis of orbital reference frames: origin and scale

In this section we analyse orbit results over the three months Oct-Nov-Dec 2002, for all six satellites, using five gravity field models: two pre-GRACE models: EGM96 and GRIM5, and three models using the GRACE observations: GFZ01S (EIGEN-GRACE), GGM01S, and GGM01C. The latter is used as a reference in the comparisons.

4.1 The data analysed

The common orbit computation strategy was the following

- Data
 - o Spot 2, Spot 4, Spot 5: DORIS only
 - o Topex/Poseidon, Jason 1, Envisat: DORIS+SLR
- References
 - o Terrestrial reference frame fixed to ITRF2000
 - o Earth orientation fixed to IERS C04
 - o Gravity fields complete to degree and order: 95, 95
- Analysis conditions
 - o Elevation cutoff: 12 °
 - o Orbit length: 24 hours
- Other estimated parameters:
 - o atmospheric drag
 - o solar pressure
 - o Hill empirical parameters
 - o Troposphere zenith delay per pass and per station
 - o frequency offset per pass and per station

The results are under the form of time series of differences between 90 daily orbits computed in ITRF2000 with four different gravity field models relative to GGM01C. Examples of these time series are shown in figures 4.1, 4.2 and 4.3.

The orbits are compared in terms of the four transformation parameters than define the offset between the origins of the frames (translations Tx, Ty and Tz) and their relative scale differences. The complete set of plots (six satellites, four pairs of gravity fields) is available at the anonymous ftp directory lareg.ensg.ign.fr/pub/martine/IDS_2004. Note the existence of two still unexplained steps in scale at mid-November 2002 (not shown here) in the differences GGM01S-GGM01C for satellites Spot5 and Jason. The magnitudes of the steps are respectively about 2 ppb and 1 ppb.

The analysis of these series presented here is deterministic as well as statistical:

- The systematic differences are modelled as a bias and a linear drift over the 90-day span. The standard deviations of the postfit residuals – labelled as “detrended standard deviation” in the graphs - are also considered.
- The stability analysis uses the Allan variance tool, described in section 2. It allows to identify three main spectral schemes: white noise, flicker noise and random walk.

Figures 4.1 through 4.3 show examples of the behaviour of the differences.

- Figure 4.1 show the translation and scale (labelled Delta) differences EGM96-GGM01C for two satellites: Spot 5 and Topex/Poseidon. The Allan graphs show a white noise spectrum, starting at 1cm for translations and 0.3 ppb in scale for the one day sampling time. The level of noise masks the effect of the linear trends, except for the larger values in Tz, that are reflected by a start of random walk at the one-month sampling time.
- Figure 4.2 show the translation and scale differences GRIM5-GGM01C and GFZ01S-GGM01C for Spot 5. The pre-GRACE GRIM5-difference signal is dominated by a trend in Tx and white noise in Ty (2mm @ 1d) and scale (0.1 ppb @ 1d); while in Tz the trend overcomes the white noise from about one week on. The differences between the two Grace models GFZ01S and GGM01C have very similar characteristics, except for the negligible trend in Tx.
- Figure 4.3 show the translation and scale differences GRIM5-GGM01C and GFZ01S-GGM01C for Jason1. The most striking effect is in the scale, where the Allan shows no improvement beyond the level 0.1 ppb @ 1d for longer sampling times. The noise pattern for the translation parameters is generally less white than for Spot 5.

4.2 Deterministic analysis of the differences

Detailed results for biases and drifts and the corresponding postfit residuals are given in the three sub-sections hereafter. Leaving aside the effect of the two scale steps mentioned above, one may summarise as follows the main characteristics of the differences.

- The gravity field dependence of the 90-day **biases** between orbit frames stay within 10 mm for the origin and 0.8 ppb for the scale. The satellite dependence is in general smaller than 2 mm / 0.1 ppb, with the exception of GRIM5 in Ty and scale.
- The gravity field dependence of the local **linear slopes** between orbit frames stay within 15 mm/90days for the origin and 0.1 ppb/90days for the scale. The satellite dependence is in general smaller than 2 mm/90days / 0.1 ppb/90days, with the exception of EGM96 in Tx and Tz.
- The gravity field dependence of the **postfit residuals** between orbit frames stay within 15 mm for the origin and 0.1 ppb for the scale. The satellite dependence is in general smaller than 2 mm / 0.1 ppb, with the exception of EGM96 in Tx and Tz.

Origin

- Differences satellite-to-satellite up to 10 mm
- $|\mathbf{T_x}| < 3 \text{ mm}$ Most satellite-dependent for GFZ01S and GGM01S
Least gravity field model dependent for Envisat
- $|\mathbf{T_y}| < 6 \text{ mm}$ Most satellite-dependent for GRIM5 and GGM01S
Most gravity field model dependent for Envisat
- $|\mathbf{T_z}| < 10 \text{ mm}$ Most satellite-dependent for EGM96 and GGM01S
Most gravity field model dependent for Envisat

Scale

- Differences satellite-to-satellite up to 0.8 ppb
- Most satellite-dependent for GRIM5 and GGM01S
- Most gravity field model dependent for Spot5
- Outliers: GGM01S/Spot5: - 0.54 ppb; GGM01S/Jason1: - 0.35 ppb

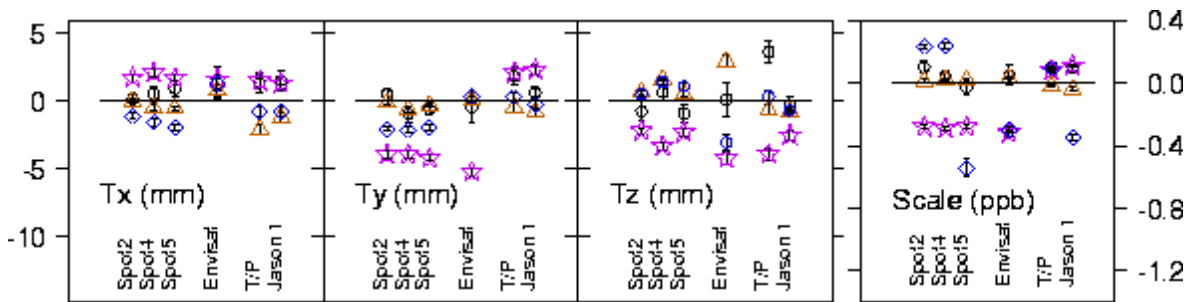


Figure 4.4. Biases of the translation parameters and scale, per satellite and gravity field: EGM96 (black open circles), GRIM5 (pink stars), GFZ01S (brown triangles), and GGM01S (blue diamond). The reference date is the middle of the data span (2002.9).

4.2.2 Local drift (over 90 days)

The effect of the change of gravity field is shown in figure 4.5 in terms of local linear drifts in the reference frame origin and in the scale. The effects may be summarised as follows.

Origin

- Differences satellite-to-satellite up to 15-20 mm/90d
- $|\mathbf{T_x}| < 15 \text{ mm}/90\text{d}$ Most satellite-dependent for EGM96 and GRIM5
Most gravity field model dependent for Spot2
- $|\mathbf{T_y}| < 8 \text{ mm}/90\text{d}$ Most satellite-dependent for GRIM5 and GGM01S
Least gravity field model dependent for Jason1
- $|\mathbf{T_z}| < 8 \text{ mm}/90\text{d}$ Most satellite-dependent for GRIM5
Most gravity field model dependent for Topex/Poseidon

Scale

- Differences satellite-to-satellite up to 0.35-0.40 ppb/90d
- Most satellite-dependent for GRIM5 and GGM01S
- Outliers: GM01S/Spot5: - 2 ppb/90d (out of scale); GM01S/Jason1: - 1 ppb/90d

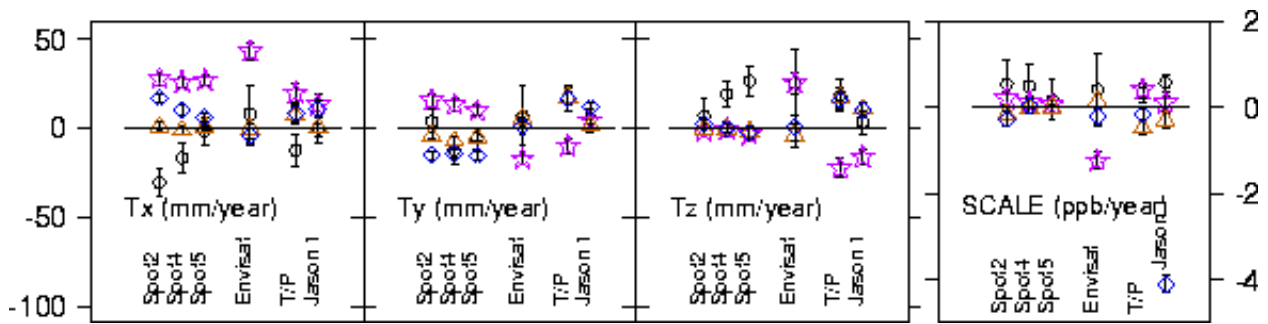


Figure 4.5. Linear drifts of the translation parameters and scale, per satellite and gravity field: EGM96 (black open circles), GRIM5 (pink stars), GFZ01S (brown triangles), and GGM01S (blue diamond).

4.2.3 Residual scattering

The effect of the change of gravity field is shown in figure 4.6 in terms of scattering in the reference frame origin and in the scale after the least squares-estimated bias and drift have been taken out. This statistics is usually referred to as “repeatability”. The effects may be summarised as follows.

Origin

- EGM96: detrended standard deviation 5-6 mm, larger for Envisat (10 mm)
- All others: detrended standard deviation < 4 mm
- Differences satellite-to-satellite are small
- Differences between gravity fields are small

Scale

- EGM96: detrended standard deviation 0.1-0.5 ppb
- All others: detrended standard deviation < 0.2 ppb
- Differences satellite-to-satellite small, except for EGM96
- Outlier: GGM01S/Spot5: 0.48 ppb

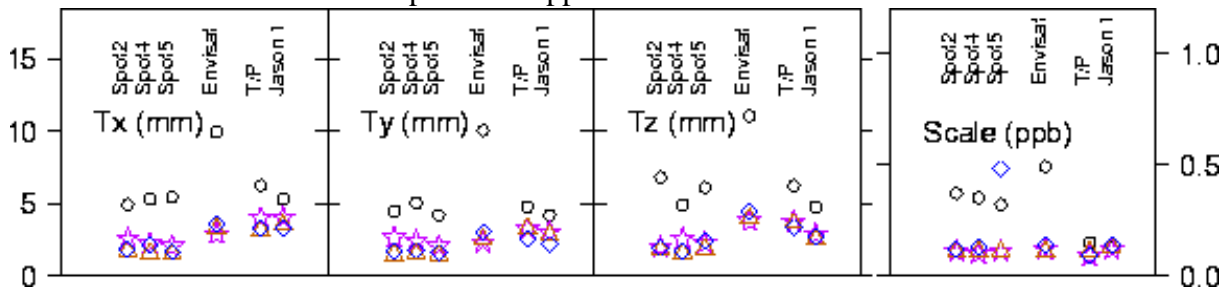


Figure 4.6. Postfit residuals of the translation parameters and scale, per satellite and gravity field: EGM96 (black open circles), GRIM5 (pink stars), GFZ01S (brown triangles), and GGM01S (blue diamond).

4.3 Spectral time analysis of differences

In this section we analyse the series of translation and scale parameters under the view point of statistical stability, using the Allan variance tool. The stability graphs are shown in figure 4.7. The effects may be summarised as follows.

Origin

- Mostly **white noise** => **< 1mm @ 1 month**
- EGM96 differences least stable (> 1 mm @ 1 month)
- Anomalous behaviours

Scale

- Mostly **white noise** => **< 0.05 ppb @ 1 month**
- EGM96 differences least stable (> 0.05 ppb @ 1 month)
- Anomalous behaviours with GRIM5 for T/P and Jason

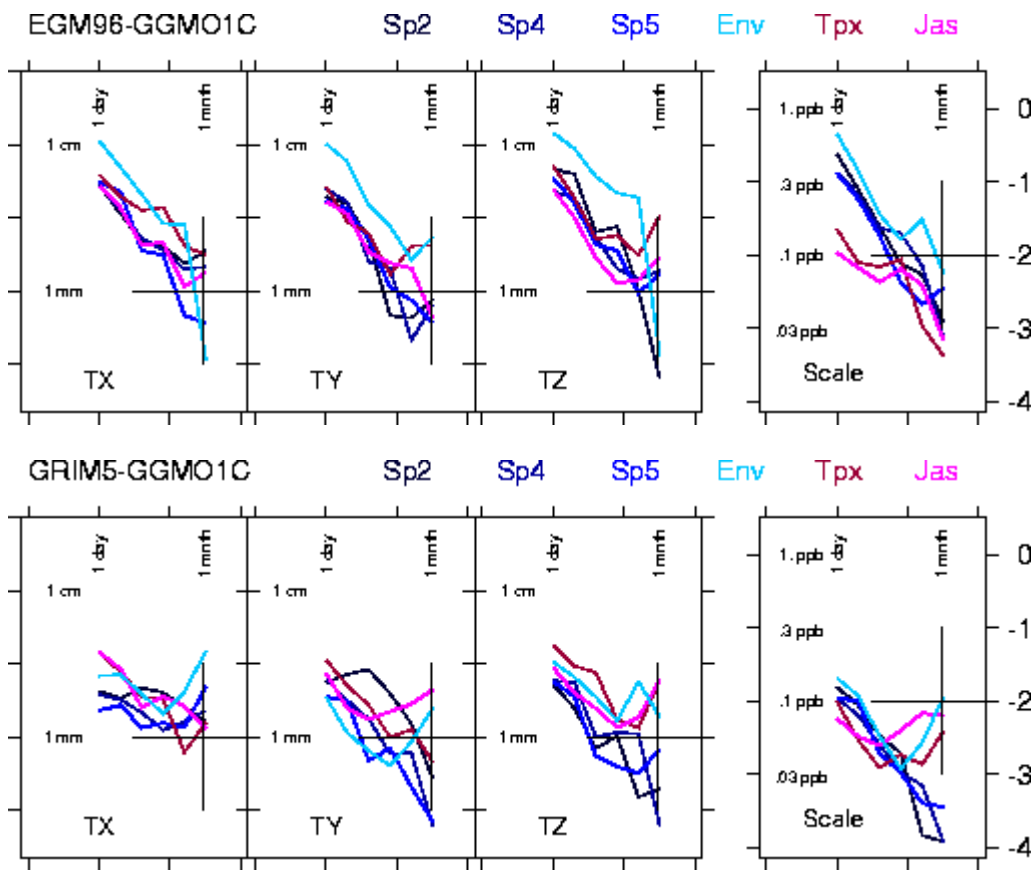


Figure 4.7. Stability graphs of the relative translation parameters and scale, per satellite and gravity field.

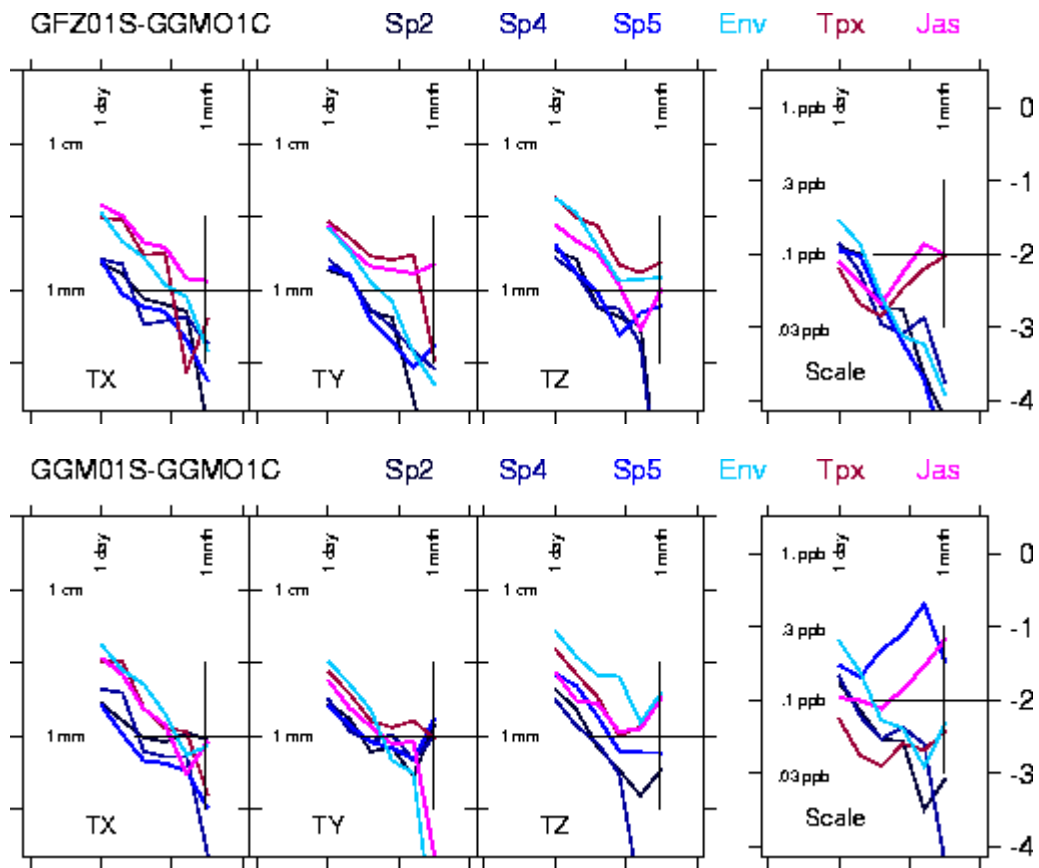


Figure 4.7 (cont). Stability graphs of the relative translation parameters and scale, per satellite and gravity field.

4.4 Global effects on the orbital and terrestrial reference frames

The origin and scale effects of the change of gravity field, averaged over all satellites except Jason1 are shown in figure 4.8. The direct biases, slopes and standard deviation of postfit residuals are listed in Tables 4.1. for all satellites except Jason 1. The origin bias and drift differences with the GGM01C-referred solutions are smaller than 1 mm and 1 mm/90d respectively, with outliers for EGM96 and GRIM5. The relative scale biases and slopes are smaller than 0.06 ppb and 0.1 ppb/90d, with the exception of GGM01S (-0.5 ppb/90d).

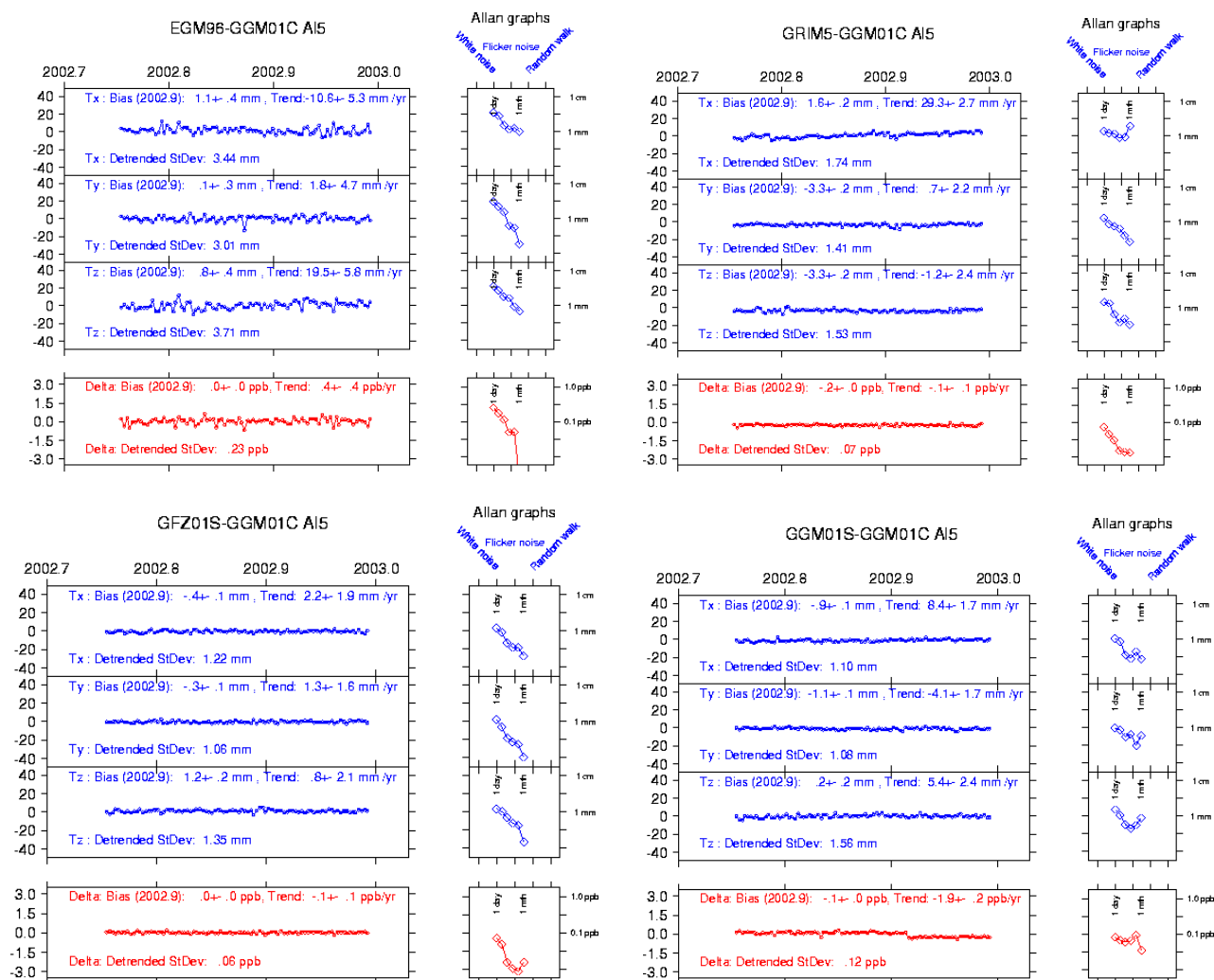


Figure 4.8. Translation and scale parameters relative to the GGM01C-based solution, averaged over the five satellites Spot2, Spot4, Spot5, Topex/Poseidon and Envisat.

Table 4.1. Multi-satellite average differences in orbital reference frames over Oct-Dec 2002 using various gravity field models. The reference solution is that using GGM01C.

Gravity Field	Tx			Ty			Tz		
	Bias	+-	Stdev	Bias	+-	Stdev	Bias	+-	Stdev
	mm	mm/year	mm	mm	mm/year	mm	mm	mm/year	mm
EGM96	1.1	0.4	3.4	0.1	0.3	3.0	0.8	0.4	3.7
GRIM5	1.6	0.2	1.7	-3.3	0.2	1.4	-3.3	0.2	1.5
GFZ01S	-0.4	0.1	1.2	-0.3	0.1	1.1	1.2	0.2	1.4
GGM01S	-0.9	0.1	1.1	-1.1	0.1	1.1	0.2	0.2	1.6

	Scale (ppb)				
	Bias	+-	Drift	+	Stdev
	ppb	ppb	ppb/year	ppb/year	ppb
EGM96	0.05	0.03	0.35	0.36	0.23
GRIM5	-0.23	0.01	-0.07	0.11	0.07
GFZ01S	0.02	0.01	-0.07	0.10	0.02
GGM01S	-0.06	0.01	-1.92	0.19	0.12

The orbital differences listed in Tables 4.1 for all satellites (except Jason 1, not used for positioning in this campaign) allow a parallel with the terrestrial reference frame differences over the same time period. Table 4.2 gives the local linear rates in orbital and terrestrial reference frames over Oct-Dec 2002. The level of agreement between the orbital and terrestrial frames slopes is at the level of 1-2 mm/90d in the equatorial plane, 4-8 mm/90d along Tz, and 0.3-3.0 ppb/90d.

Table 4.2. Relative linear rates over Oct-Dec 2003 in orbital and terrestrial reference frames, referred to EGM96

Analysis Center	Reference frame	Comparison Grav. Field	Tx mm/year	Ty mm/year	Tz mm/year	scale ppb/year
lca	orbital	GGM01C	-10.6 ± 5.3	+1.8 ± 4.7	+19.5 ± 5.8	+0.35 ± 0.36
lca	terrestrial	GFZ01S	-17.0	+11.7	-9.9	-11.0
ign	terrestrial	GGM01C	-10.9	+4.8	+3.7	+1.1

5. Summary: sensitivity to gravity field and to analysis environment

Time series of DORIS-derived terrestrial reference frames obtained by three IDS Analysis Centers (IGN_JPL, LEGOS-CLS, INASAN) using six Earth gravity field models (JGM3, EGM96, GRIM5, GGM01S, GGM01C, EIGEN-GRACE01) were analysed and compared.

The investigations are based on the standard analysis tools of the IDS Analysis Coordinator team: CATREF for the ITRF referencing of series of unconstrained series of SINEX TRF files; Crono_Vue for the extraction of seasonalities and trend, Allan variance analysis to spectrally describe time series of measurements. The parameters analysed are the station coordinates, the origin and scale of the terrestrial reference frames (TRF), origin and scale of the satellite orbital planes.

5.1 Short term internal consistency of station coordinates

A first comment concerns the improvement of results with increasing number of satellites. Starting with 2002, when five satellites are available (Spot 2, 4, 5, Topex/Poseidon and Envisat), the coordinates consistency within one week solution reaches 15 mm. This represents an improvement by a factor of two with respect to the earlier results.

Short term coordinates consistency. Over Oct-Dec 2002, the average coordinate consistency within one week improves from 21 mm to 16 mm for IGN-JPL when replacing EGM96 by GGM01C in the DORIS data analysis. For LEGOS-CLS, this consistency stays between 13 and 17 mm for the five gravity field models tested. The best performance is obtained using GGM01S.

5.2 Terrestrial reference frame sensitivity to the analysis context

Short term scattering in origin and scale. The scattering of the weekly TRF origin coordinates and scale after taking out a bias, an annual term and a linear trend is 6 mm in Tx and Ty, 19 mm in Tz and 0.6 ppb in scale.

Medium term effects in origin and scale. The effect of the gravity field used on the behaviour of these parameters over Oct-Dec 2002 is insignificant when compared with the differences between Analysis Centers.

Seasonal components in origin and scale. We find insignificant differences associated with the change of gravity field in the measured motion of *the TRF origin in the equatorial plane* (2 mm and 0.1 ppb, respectively) and a reasonable agreement in phase and amplitude of the DORIS results with the geophysical prediction before 1999. Note that the amplitude of the DORIS Tx signal increases continuously in time. Whether this varying amplitude shows real physical variations, or it reflects time varying systematic errors remains to be understood. In *Tz*, the annual component is much larger than the geophysical expectation. It is not influenced by the reference gravity field. The IGN-JPL and LEGOS-CLS components are in phase, the LEGOS-CLS amplitude being about half of the IGN-JPL one. The *scale* has a marked seasonal variation in the IGN-JPL solution (0.8 ppb peak-to-peak), slightly varying in time but unaffected by the gravity field model. The LEGOS-CLS seasonal component is smaller (0.1-0.5 ppb peak-to-peak) and somewhat unstable.

Interannual and long term variations in origin and scale. The effect of the gravity field on the long term TRF origin motion is negligible when compared to the differences between the Analysis Centers. One striking exception is the presence of differences up to 3 ppb in the interannual *Tz* component of the IGN-JPL solutions referred to EGM96 and GGM01C (figure 3.4).

Spectral characteristics of the TRF origin and scale variations. These parameters have similar spectral characteristics for all three Analysis Centers: The annual signatures are imbedded in noise, at the level of 4 mm in Tx and Ty, 8-12 mm in Tz and 0.3-1.0 ppb in scale. The background spectrum in the origin motion is that of flicker noise regardless of the gravity field in the case of IGN-JPL, and white noise in the cases of INASAN and LEGOS-CLS. For the scale, the background of the IGN-JPL and INASAN solutions is white noise, with a slightly better long term stability for the IGN-JPL solution referred to GGM01C. The noise level is around 0.3 ppb for a one-year sampling time. The background spectrum in the LEGOS-CLS solution is that of flicker noise at the 0.5 ppb level.

TRF scale bias. The systematic differences, at the level of several ppb, in the DORIS TRF scales already mentioned in the ITRF2000 analysis (Boucher et al. 2004) are confirmed. They are unaffected by the change in gravity fields.

5.3 Orbital reference sensitivity to the gravity field model used

The results analysed are differences of orbits referred to EGM96, GRIM5, EIGEN-GRACE01S and GGM01S with those referred GGM01C. The parameters considered are series of relative daily origin coordinates and scales of the orbital references.

Orbital reference origin and scale: systematic differences. The systematic differences are expressed as biases over the 90-day time span of the data. The differences in the origins are smaller than 6 mm in the equatorial plane and 10 mm in Tz. The scale differences are smaller than 0.8 ppb. The differences are most satellite dependent for GRIM5 and GGM01S, then EGM96, and most gravity field dependent for Envisat in origin and Spot5 in scale.

Orbital reference origin and scale: short term sensitivity. The standard deviation of the short term differences stay in general under 4 mm in the origin and 0.2 ppb in scale, except for EGM96, where they are larger. Note one outlier in scale: GGM01S/Spot5 (0.5 ppb).

Orbital plane origin and scale: medium term variations. The medium term effects are investigated under the form of drift of the origin and scale over the 90-day the data span. The differences are at the level of 10mm/90d in origin and 0.4 ppb/90d in scale. They are most satellite dependent for GRIM5, then EGM96 and GGM01S, most gravity field dependent for Spot2 and Topex/Poseidon, and least gravity field dependent for Jason1.

Spectral characteristics of the orbital plane origin and scale. The origin and scale times series of differences have a white noise spectrum, reaching a stability level better than 1mm and 0.05 ppb for a one-month sampling time. Some anomalous behaviours are noted.

Global orbital and terrestrial frame effects. The differences of the local rates over Oct-Dec 2002 in the orbital and terrestrial frames for solutions referred to Grace gravity fields relative to those referred to EGM96, show agreement at the level of 1-2 mm/90d in the equatorial plane and 4-8 mm/90d along Tz. The scale discrepancies may reach 3.0 ppb/90d.

6. Conclusion

The initial aim of this analysis campaign was to evaluate the impact of the advent of Earth gravity field models derived from the GRACE mission on DORIS-derived positioning and terrestrial reference frame. Thanks to the availability of daily orbital reference comparisons, the study could be extended to orbital references through their origin and scale. In addition, the availability of four long time series from three Analysis Centers made it possible to evaluate the analyst related differences.

The major anomalies in the measured motion of the TRF origin are discrepant amplitudes of the annual components in Tz between Analysis Centers (10 mm) and with respect to the geophysical expectation (5-15 mm). The annual component in Tx is in agreement between Analysis Centers but its amplitude increases in time, which does seem to be the case for the geophysical expectation. The interannual TRF origin motion differences between solutions reach up to 3 mm, maybe related to the gravity field model in one case.

The TRF scale differences between Analysis Centers have a complex signature, including drifts (0.6 ppb/year), biases (6 ppb), interannual (0.3 ppb) and annual (0.5 ppb) components. These are probably due to differences in modelling still to be understood.

The study of the influence of the gravity field on the orbital reference frame was studied on three-month time span with results from one Analysis Center, LEGOS-CLS. The short term sensitivity to the change in gravity field is at the level of 4 mm on the origin and 0.2 ppb in scale. The medium term variations reach 10 mm/90d and 0.4 ppb/90d, which is somewhat larger than the annual effect on the terrestrial reference frames. The spectral investigation of the series of differences leads to a global white noise diagnostic, ruling out the presence of significant perturbations at long periods with respect to the 90-day data span.

Finally, parallel comparisons of terrestrial and orbital reference frames, based on either EIGEN-GRACE01, GGM01S or GGM01C, to those based on EGM96 show modest medium term differences in the frame origins (2 mm/90d in Tx, Ty, and 4-8 mm/90d in Tz) and quite large effects in scale (3 ppb/90d).

Annex 1. Allan variance response to simulated signals

We present hereafter numerical simulations showing the response of the Allan variance analysis to various mixed noises. Figures 1 through 3 show the Allan variance signatures of various mixes of white noise, flicker noise and random walk, in logarithmic scales. The variances of the three generated signals are equal to each other. They are symbolised on the Allan graph by an open circle. Note that the classical variance of the signal is equal to the integral of the Allan variances over the series of sampling times. The Allan graph of the resulting signal is the sum of the components' graphs. Thus, the level of the most unstable components eventually dominates the spectrum as sampling times get larger and larger.

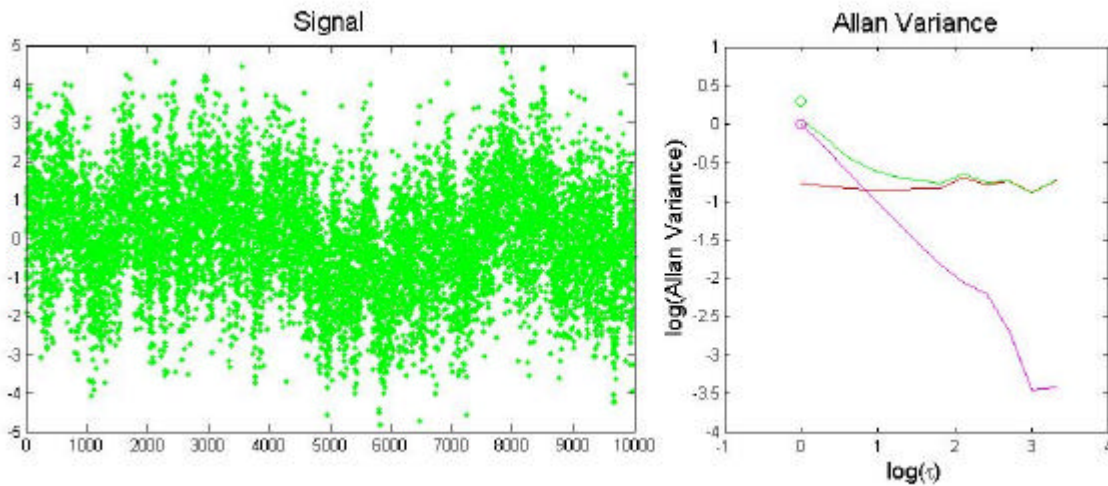


Figure 1. Allan variance of mixed noises: white noise + flicker noise. The graph on the right shows the resulting signal. The graph on the left gives the Allan variance graph of the two components, with slopes -1 for the white noise (pink) and 0 for the flicker noise (red). The two components have the same variance, shown by the pink open circle. The Allan graphs and variance of the resulting signal are plotted in green.

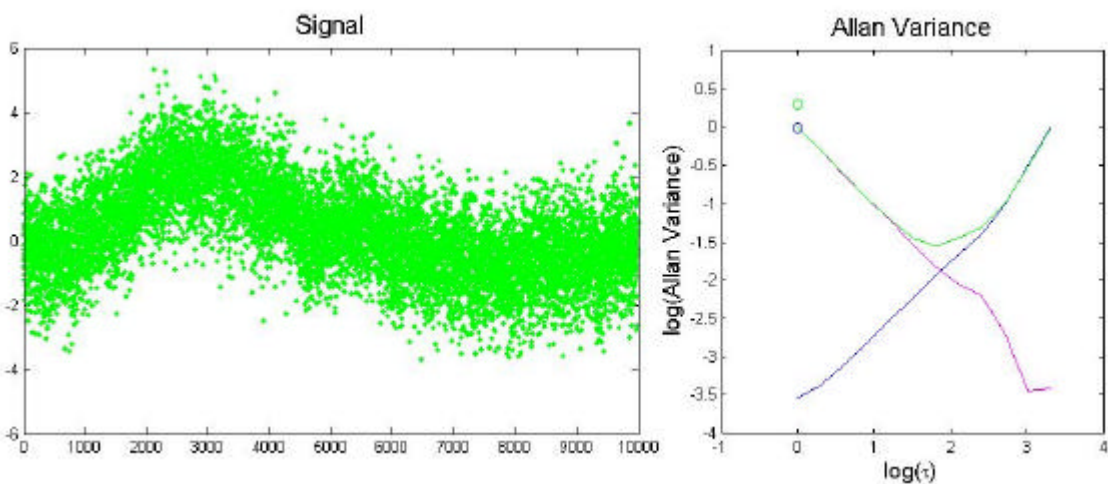


Figure 2. Allan variance of mixed noises: white noise + random walk. The graph on the right shows the resulting signal. The graph on the left gives the Allan variance graph of the two components, with slopes -1 for the white noise (pink) and $+1$ for the random walk (blue). The two components have the same variance, shown by the blue open circle. The Allan graphs and variance of the resulting signal are plotted in green.

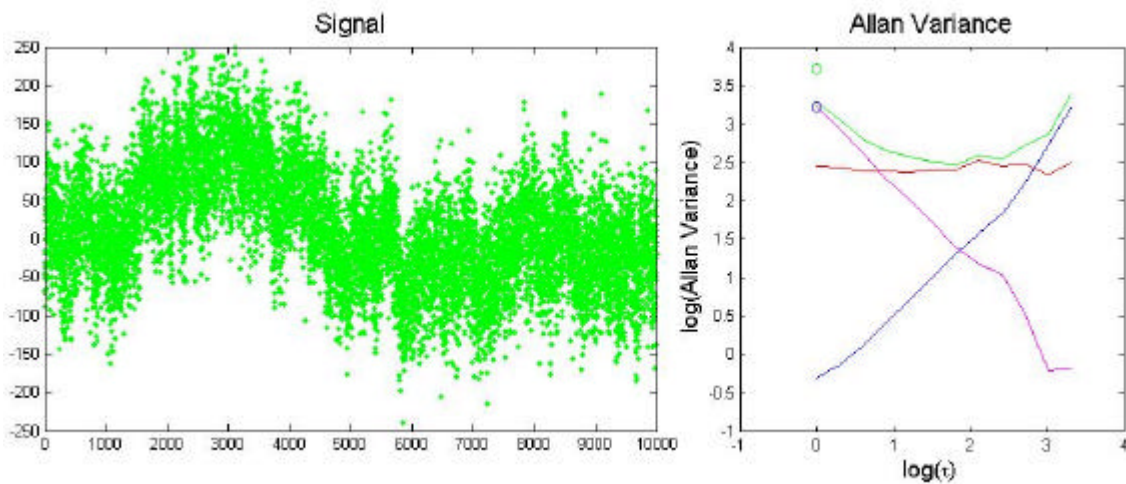


Figure 3. Allan variance of mixed noises: white noise + flicker noise + random walk. The graph on the right shows the resulting signal. The graph on the left gives the Allan variance graph of the three components, with slopes -1 for the white noise (pink), 0 for the flicker noise (red), and $+1$ for the random walk (blue). The two components have the same variance, shown by the blue open circle. The Allan graphs and variance of the resulting signal are plotted in green.

Figures 4 and 5 show the Allan variance signatures when a periodic component is added to white noise. The signature of the periodic component is a dip when the sampling time matches the period. The influence of the periodic component fades out as sampling times get larger and larger.

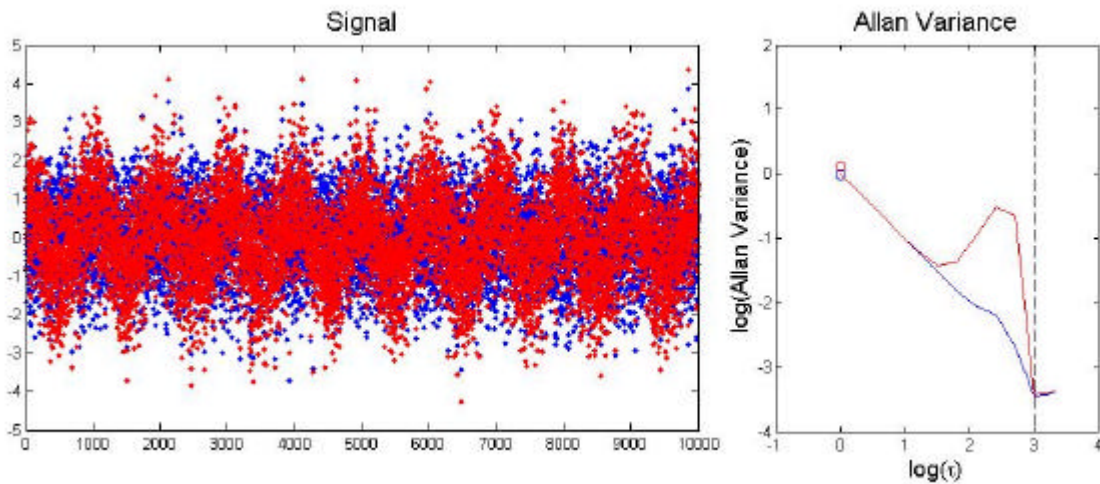


Figure 4. Allan variance of mixed signal and noise: white noise + periodic term at similar level. The graph on the right shows the two components of the signal. The graph on the left gives the Allan variance graph of the white noise alone in blue and that of the mixed signal in red. The open circles show the variances of these two signals. The vertical line shows the period of the periodic components (1000 times the tabular interval).

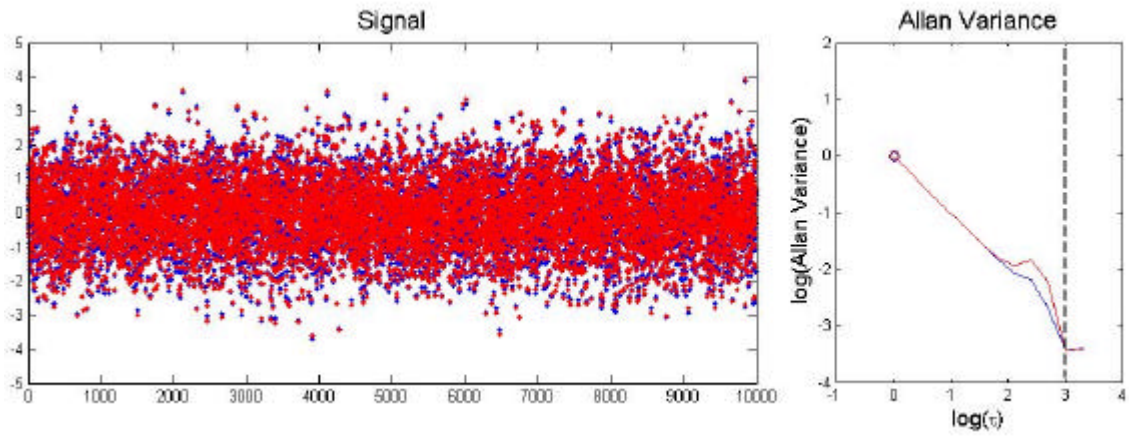


Figure 5. Allan variance of mixed signal and noise: white noise + weak periodic term. The graph on the right shows the two components of the signal. The graph on the left gives the Allan variance graph of the white noise alone in blue, and that of the mixed signal in red. The open circles show the variances of these two signals. The vertical line shows the period of the periodic components (1000 times the tabular interval).

Annex 2. References and acknowledgement

Allan, D.W. 1966, Proc. IEEE 54, 221

Altamimi Z., P. Sillard and C. Boucher, 2002. ITRF2000: a new release of the International Terrestrial Reference Frame for earth science applications, JGRB., 107

Altamimi Z., C. Boucher and P. Sillard, 2001. New Trends for the Realization of the International Terrestrial Reference System, Adv. Space Res., 30, 175

Boucher, C., Altamimi, Z., Sillard, P., Feissel-Vernier, M., 2004. The ITRF 2000. IERS Technical Note No. 31.

IERS, 2003, <ftp://alpha.fesg.tu-muenchen.de/iers/sinex/format/>

Sillard P. and C. Boucher – A review of algebraic constraints in terrestrial reference frame datum definition. J. Geodesy 75: 63-73, 2001.

Feissel-Vernier, M., G. Ramillien, K. Le Bail, J.-J. Valette, 2004. Geodetic and geophysical use of geocenter time series. COSPAR 2004 Assembly, Session PSD1/B2.1. Paris July 2004.

Rutman, J., 1978, Proc. IEEE 66, 1048

Acknowledgement. We thank Z. Altamimi (IGN/LAREG) for giving access to the CATREF software and for giving advice on its optimal use.